Anal. Chem. **2007,** *79,* 7291−7300

Continuous-Flow Particle Separation by 3D Insulative Dielectrophoresis Using Coherently Shaped, dc-Biased, ac Electric Fields

Benjamin G. Hawkins,† A. Ezekiel Smith,‡ Yusef A. Syed,§ and Brian J. Kirby*,§

Department of Biomedical Engineering, School of Applied and Engineering Physics, and Sibley School of Mechanical & Aerospace Engineering, College of Engineering, Cornell University, Ithaca, New York 14853

We present the development of a continuous-flow, "dielectrophoretic spectrometer" based on insulative DEP techniques and three-dimensional geometric design. Hot-embossed thermoplastic devices allow for high-throughput analysis and geometric control of electric fields via ridged microstructures patterned in a high width-to-depth aspect ratio (250:1) channel. We manipulate particles with dc-biased, ac electric fields and generate continuous-output streams of particles with a transverse outlet position specified by linear and nonlinear particle mobilities. We show, with simulation and experiment, that characteristic shape factors can be defined that capture the effects of constrictions in channel depth and that modulating the angle of these constrictions changes the resulting local DEP force. Microdevices are fabricated with an insulative constriction in channel depth, whose angle of incidence with the direction of flow varies continuously across the channel width. The resulting electric field gradients enable demonstration of a dielectrophoretic spectrometer that separates particles and controls their transverse channel position.

Dielectrophoresis (DEP)-based techniques offer a number of significant advantages over traditional methods for particle separation such as FACS, flow cytometry, ELISA, and affinity chromatography. The dielectrophoretic force—force on a dipole due to electric field gradients[1,2]—requires no secondary affinity coupling steps to achieve continuous-flow separation, because it is a direct function of particle characteristics such as size, charge, conductivity, and permittivity. When applied to cells, the DEP force is a direct function of these parameters, thus defining a cell's "electrical phenotype".[3] This character makes DEP especially useful for effecting separation of cells based on size, species, growth cycle, viability, and phenotype. Phenotypic discrimination of cellular analytes is a necessary step in many drug development and biological research protocols. Discrimination of cells based on membrane phenotype is particularly critical for bacterial species whose pathogenicity is closely tied to membrane composition, such as existing and emerging strains of *Mycobacterium tuberculosis*, as well as *Mycobacterium avium* complex.[4] At present, discrimination and separation based on membrane phenotype in *Mycobacterium* species is primarily accomplished by direct visual inspection.

Electrode-based dielectrophoretic techniques (eDEP) are the most widely used. Electrodes create high electric fields and field gradients with a relatively low applied potential and are compatible with high ($>10^4$ Hz) frequency operation, for which electrolysis can be managed.[5−17] Electrode geometries are defined by lithographic processes, and therefore, numerous planar electrode configurations exist. While offering flexibility in electrode geometry, linear electrokinetic actuation of fluid and particles through dc electroosmosis and electrophoresis is not generally possible, due to the generation of electrolytic products.

Electrodeless or insulative DEP (iDEP) techniques are becoming more widely used because they can be actuated with both ac and dc electric fields, can be used at low frequencies in solutions

* To whom correspondence should be addressed. E-mail: bk88@cornell.edu; Phone: 6072554379.

† Department of Biomedical Engineering.

‡ School of Applied and Engineering Physics.

§ Sibley School of Mechanical & Aerospace Engineering.

(1) Pohl, H. A. *Dielectrophoresis: The behavior of neutral matter in nonuniform electric fields*; Cambridge University Press: Cambridge, UK, 1978.

(2) Jones, T. B. *Electromechanics of Particles*; Cambridge University Press: Cambridge, UK, 1995.

(3) Voldman, J. *Annu. Rev. Biomed. Eng.* **2006**, *8*, 425−454.

(4) Rhoades, E. R.; Geisel, R. E.; Butcher, B. A.; McDonough, S.; Russell, D. G. *Tuberculosis* **2005**, *85*, 159−176.

(5) Fiedler, S.; Shirley, S. G.; Schnelle, T.; Fuhr, G. *Anal. Chem.* **1998**, *70* (9), 1909−1915.

(6) Fuhr, G.; Arnold, W. M.; Hagedorn, R.; Muller, T.; Benecke, W.; Wagner, B.; Zimmermann, U. *Biochim. Biophys. Acta* **1992**, *1108* (2), 215−23.

(7) Fuhr, G.; Glasser, H.; Mueller, T.; Schnelle, T. *Biochim. Biophys. Acta* **1994**, *1201* (3), 353−360.

(8) Fuhr, G.; Hagedorn, R.; Mueller, T.; Schnelle, T. Microelectrode arrangements for production of functional field barriers during dielectrophoresis, European patent DE19860118. 2000.

(9) Fuhr, G.; Muller, T.; Baukloh, V.; Lucas, K. *Hum. Reprod.* **1998**, *13* (1), 136−41.

(10) Muller, T.; Gradl, G.; Howitz, S.; Shirley, S.; Schnelle, Th.; Fuhr, G. A *Biosens. Bioelectron.* **1999**, *14* (3), 247−256.

(11) Voldman, J. *BioMEMS Biomed. Nanotechnol.* **2006**, *4*, 159−186.

(12) Voldman, J.; Toner, M.; Gray, M. L.; Schmidt, M. A. *J. Electrostat.* **2003**, *57* (1), 69−90.

(13) Voldman, J.; Braff, R. A.; Toner, M.; Gray, M. L.; Schmidt, M. A. *Biophys. J.* **2001**, *80* (1), 531−541.

(14) Gascoyne, P.; Satayavivad, J.; Ruchirawat, M. *Acta Trop.* **2004**, *89* (3), 357−369.

(15) Gascoyne, P. R. C.; Vykoukal, J. *Electrophoresis* **2002**, *23* (13), 1973−1983.

(16) Liang, E.; Smith, R. L.; Clague, D. S.*Phys. Rev. E* **2004**, *70* (6), 1−8.

(17) Richter, E.; Fuhr, G.; Mueller, T.; Shirley, S.; Rogaschewski, S.; Reimer, K.; Dell, C. *J. Mater. Sci.: Mater. Med.* **1996**, *7* (2), 85−97.

10.1021/ac0707277 CCC: $37.00
Published on Web 09/01/2007

of physiological salinity (because electrodes are placed in external reservoirs, where electrolytic products can easily escape), and are compatible with high-volume manufacturing techniques such as injection molding. iDEP techniques use constrictions in the electrical current path to change the electric field.

The majority of eDEP and iDEP techniques reported to date are batch process techniques, which ultimately limit device throughput. Reported continuous-flow techniques[18−23] show considerable promise for rapid separation, filtering, or screening applications, but typically result in binary separations centered around a single value of DEP mobility (or ratio of mobilities[20,21]).

In this work, we introduce a device design that incorporates a curved constriction in channel depth, coupling DEP effects to transverse channel position, and use a dc-offset, ac electric field to independently control linear and nonlinear electrokinetic effects. We show that a simplified electrokinetic model adequately describes particle behavior and that continuous-flow particle separation in our device is sensitive to DEP mobility. We overcome the limitations of traditional iDEP by (i) applying a dc-offset, ac electric field to decouple linear and nonlinear electrokinetic effects, (ii) rationally designing insulative structures to actuate nonlinear forces, and (iii) noting that samples of interest respond to low-frequency applied fields. The output particle separation in our device exhibits continuous variation of dielectrophoretic mobility perpendicular to the direction of flow.

THEORY AND SYSTEM DESIGN

Most iDEP devices trap particles by countering bulk particle motion (the result of electroosmosis, electrophoresis, or pressure-driven flow) with local, dielectrophoretic forces, creating a point where the net particle velocity is zero. Insulating constrictions in the width of a microfluidic channel are traditionally used to modulate local DEP forces.[18,19,24]

Constricting the depth of a channel (rather than the width) introduces an additional degree of freedom: the angle of incidence between bulk migratory forces and opposing DEP forces. Extending this idea further, we vary the angle of incidence continuously across the channel width, transverse to the direction of flow, by using a curved constriction in depth (Figure 1).

The path of a particle through this system is governed by the relative magnitudes of electrophoretic, electroosmotic, and dielectrophoretic forces. A particle far upstream of the constriction in depth is carried along by electroosmotic fluid flow and electrophoretic particle transport. As a the particle approaches the constriction or ridge, DEP forces are applied perpendicular to the constriction (nDEP dominates for our particles at low field frequencies, which we assert in the section Nonlinear Electrokinetics). Depending on the ratio of linear to nonlinear forces, the particle will either pass the ridge or be deflected by the ridge. In the case of a trapped particle, the net velocity will be tangent to the ridge. As the trapped particle moves tangent to the ridge, the angle of incidence changes, and the ratio of linear to nonlinear forces changes. Eventually, the particle will pass the ridge, at a point determined by the ratio of a particle's characteristic linear and nonlinear mobilities.

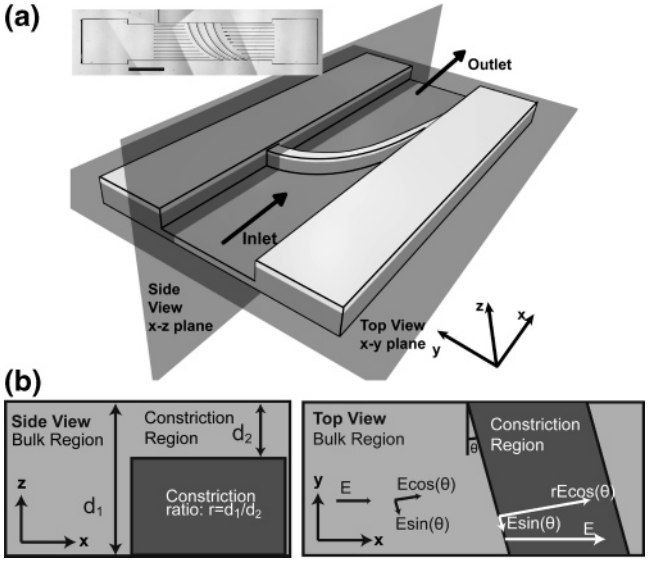

Figure 1. (a) 3D schematic of channel geometry. In (b), we define relevant geometric factors based on cross sections of the constriction region along the $x-y$ and $x-z$ planes.

To mathematically describe this behavior, we present simplified, 3D mobility models for the dominant electrokinetic phenomena: electroosmotic flow, electrophoresis of particles, and dielectrophoresis of particles. These phenomena are actuated by a dc-offset, ac electric field with a single ac frequency, ω_0 (eq 2).

$$\alpha = \frac{|\vec{E}_{ac}|}{|\vec{E}_{dc}|} \tag{1}$$

$$\vec{E} = \mathscr{R}[\vec{E}_{dc} + \vec{E}_{ac}e^{\mathbf{i}\omega_0 t}] = \mathscr{R}[\vec{E}_{dc}(1 + \alpha e^{\mathbf{i}\omega_0 t})] \tag{2}$$

where α is the ratio of ac to dc electric field amplitudes, $\mathscr{R}[x]$ denotes the real part of x, $\mathbf{i}$ is $-1^{1/2}$, and $\vec{E}$ describes the spatial variation of the electric field specified by voltage applied to reservoirs.

The mobility relationships that we use to describe theoretical particle motion are predicated on three main assumptions: thermal motion is small compared to other particle velocity components and can therefore be neglected, particles reach terminal velocity almost instantaneously, and ion concentrations can be described by Boltzmann statistics with a characteristic decay length (characterizing the double layer thickness) that is small compared to particle and channel dimensions.

Linear Electrokinetics. Electroosmosis is the bulk flow of fluid owing to the motion of mobile ions in the double layer, induced by the application of an external electric field. Assuming (i) that the double layer thickness is small compared to characteristic channel dimensions and (ii) that ion distributions can be

(18) Kang, K. H.; Kang, Y.; Xuan, X.; Li, D. *Electrophoresis* **2006**, *27*, 694−702.
(19) Kang, K. H.; Xuan, X.; Kang, Y.; Li, D. *J. Appl. Phys.* **2006**, 99.
(20) Barrett, L. M.; Skulan, A. J.; Singh, A. K.; Cummings, E. B.; Fiechtner, G. J. *Anal. Chem.* **2005**, *77*, 6798−6804.
(21) Barrett, L. M.; Skulan, A. J.; Cummings, E. B.; Singh, A. K.; Fiechtner, G. J. Insulator-based ridges for the manipulation of particles and cells in microchannels. In *Proceedings: MicroTAS 2005*; Harrison, D. J., Voldman, J., Jensen, K. F., Han, J., Eds.; Transducer Research Foundation, Inc.: Boston, MA, 2005; Vol. 2, pp 1404−1406.
(22) Cummings, E. B. *IEEE Eng. Med. Biol. Mag.* **2003**, *22* (6), 75−84.
(23) Kralj, J. G.; Lis, M. T. W.; Schmidt, M. A.; Jensen, K. F. *Anal. Chem.* **2006**, *78*, 5019−5025.
(24) Mela, P.; van den Berg, A.; Fintschenko, Y.; Cummings, E. B.; Simmons, B. A.; Kirby, B. J. *Electrophoresis* **2005**, *26* (9), 1792−1799.

described by Boltzmann statistics, we obtain the following result to describe the velocity of fluid outside the double layer:[25]

$$\vec{u}_{\mathrm{EO,bulk}} = -\frac{\epsilon_{\mathrm{m}}\zeta}{\eta}\vec{E} = \mu_{\mathrm{EO}}\vec{E} \tag{3}$$

Equation 3 defines the electrokinetic potential, ζ, and an electroosmotic mobility, μ_{EO}, each of which is dependent on the properties of the fluid and the interface between fluid and channel.

Electrophoresis is the motion of particles induced by the application of an external electric field. Applying the same assumptions as above, with the additional condition that a particle reaches terminal velocity against Stokes drag instantaneously, we find[25]

$$\vec{u}_{\mathrm{EP}} = \frac{\epsilon_{\mathrm{m}}\zeta_{\mathrm{p}}}{\eta}\vec{E} = \mu_{\mathrm{EP}}\vec{E} \tag{4}$$

Equation 4 defines electrokinetic potential, ζ_{p}, and an electrophoretic mobility, μ_{EP}, each of which is dependent on the properties of the fluid and the interface between fluid and particle.

Nonlinear Electrokinetics. Dielectrophoresis refers to the movement of particles as a result of induced or intrinsic particle and fluid multipoles interacting with a nonuniform electric field. We use a dipole approximation and neglect higher order terms in the multipole expansion. We can describe the force on an electric dipole

$$\vec{F} = (\vec{p}\cdot\nabla)\vec{E} \tag{5}$$

using an effective dipole moment vector. For a homogeneous sphere in a semi-infinite, continuous fluid domain under the influence of a quasi-static, external electric field as described by eq 1, we can determine an effective dipole moment, p_{eff}:[1,2]

$$\vec{p}_{\mathrm{eff}} = 4\pi\epsilon_{\mathrm{m}}a^3\mathscr{R}[f_{\mathrm{CM,dc}}\vec{E}_{\mathrm{dc}} + f_{\mathrm{CM,ac}}\vec{E}_{\mathrm{ac}}e^{\mathbf{i}\omega_0 t}] \tag{6}$$

$$f_{\mathrm{CM}} = \frac{\epsilon_{\mathrm{p}}^* - \epsilon_{\mathrm{m}}^*}{\epsilon_{\mathrm{p}}^* + 2\epsilon_{\mathrm{m}}^*} \tag{7}$$

$$\epsilon^* \equiv \epsilon - \frac{\mathbf{i}\sigma}{\omega} \tag{8}$$

Asterisks in the definition of the Clausius−Mossotti factor, f_{CM}, denote the use of complex permittivities as defined in eq 8.[1] The applied electric fields in our simulations and experiment are small in magnitude and frequency such that, as in eq 6, we assume frequency-independent values of permittivity, ϵ, and conductivity, σ, and consider interfacial polarization as a function of complex permittivity,[1] ϵ^*. By combining this effective dipole moment with the equation for force on a dipole in an electric field, we obtain[2]

$$\vec{F}_{\mathrm{DEP}} = 4\pi\epsilon_{\mathrm{m}}a^3\mathscr{R}[f_{\mathrm{CM,dc}}\vec{E}_{\mathrm{dc}} + f_{\mathrm{CM,ac}}\vec{E}_{\mathrm{ac}}e^{\mathbf{i}\omega_0 t}]\cdot\nabla(\mathscr{R}[\vec{E}_{\mathrm{dc}} + \vec{E}_{\mathrm{ac}}e^{\mathbf{i}\omega_0 t}]) \tag{9}$$

Evaluating this expression leads to both oscillatory terms (at ω and 2ω) as well as constant (dc) terms. Assuming (as is the case for our experiments) that the ac electric field frequency is low (1 kHz is used in here in simulation and experiment), then $f_{\mathrm{CM,ac}} \approx f_{\mathrm{CM,dc}}$.

Observed particle motion is the result of the time-averaged force. The expectation values for the average forces due to electroosmosis and electrophoresis are dependent only on the constant component of the electric field, E_{dc}. For DEP, we define the ac to dc ratio as α (eq 1), integrate the DEP force over one period of oscillation, and find

$$\langle\vec{F}_{\mathrm{DEP}}\rangle = (\alpha^2 + 2)\pi\epsilon_{\mathrm{m}}a^3\mathscr{R}[f_{\mathrm{CM}}]\nabla(|\vec{E}_{\mathrm{dc}}|^2) \tag{10}$$

Equation 10 is cast in terms of a dc electric field and an ac to dc ratio in anticipation of experimental results to follow. The Reynolds number based on the characteristic size of the particle is $\ll 1$, implying Stokes flow. The terminal velocity due to dielectrophoretic forces is thus found by balancing F_{DEP} with the typical formulation for Stokes drag (eq 11), resulting in a definition for the DEP mobility, μ_{DEP}:

$$\vec{u}_{\mathrm{DEP}} = (\alpha^2 + 2)\frac{\epsilon_{\mathrm{m}}a^2\mathscr{R}[f_{\mathrm{CM}}]}{6\eta}\nabla(|\vec{E}_{\mathrm{dc}}|^2)$$

$$\vec{u}_{\mathrm{DEP}} = (\alpha^2 + 2)\mu_{\mathrm{DEP}}\nabla(|\vec{E}_{\mathrm{dc}}|^2) \tag{11}$$

While DEP is most often associated with ac fields, it should be noted that the dielectrophoretic velocity has contributions from both ac and dc electric fields (while still assuming that $f_{\mathrm{CM,ac}} \approx f_{\mathrm{CM,dc}}$ as above). The dc component of DEP can be illustrated by setting the ac to dc ratio to zero:

$$\alpha = 0 \Rightarrow \vec{u}_{\mathrm{DEP}} = 2\mu_{\mathrm{DEP}}\nabla(|\vec{E}_{\mathrm{dc}}|^2) \tag{12}$$

Particle Transport. We have cast electrokinetic velocity components in terms of characteristic mobilities, which we will refer to exclusively throughout the remainder of this paper.

$$\vec{u} = \vec{u}_{\mathrm{DEP}} + \vec{u}_{\mathrm{EO}} + \vec{u}_{\mathrm{EP}}$$

$$\vec{u} = \mu_{\mathrm{DEP}}\nabla(\vec{E}\cdot\vec{E}) + (\mu_{\mathrm{EO}} + \mu_{\mathrm{EP}})\vec{E} \tag{13}$$

The above equation is composed of both (i) terms dependent on the linear electric field and (ii) a nonlinear term dependent on the gradient of the squared electric field. The first-order dependence of electroosmosis and electrophoresis on $\vec{E}_{\mathrm{dc}}$ leads us to refer to these effects as "linear electromigatory effects". Similarly, the second-order dependence of dielectrophoresis on $\vec{E}_{\mathrm{dc}}$ leads us to refer to it as a "nonlinear electromigratory effect". From eq 13, it can be seen that particle velocity is dependent on the DEP, EO, and EP mobilities; the electric field; the gradient of the electric field squared; and the ac to dc ratio α. Inserting the average DEP velocity, we obtain

(25) Probstein, R. F. *Physicochemical Hydrodynamics,* 2nd ed.; Wiley-Interscience: New York, 1994.

$$\vec{u} = (\alpha^2 + 2)\mu_{DEP}\nabla(|E_{dc}|^2) + (\mu_{EO} + \mu_{EP})\vec{E}_{dc} \quad (14)$$

Examining the high- and low-frequency limits of this equation, we recover the expected relationships for particle dielectrophoretic behavior:

$$\lim_{\alpha\to 0}\vec{u} = 2\mu_{DEP}\nabla(|E_{dc}|^2) + (\mu_{EO} + \mu_{EP})\vec{E}_{dc} \quad (15)$$

$$\lim_{\alpha\to\infty}\vec{u} = 2\mu_{DEP}\nabla\left(\frac{\alpha^2}{2}\left|E_{dc}\right|^2\right) = 2\mu_{DEP}\nabla(|E_{ac,rms}|^2) \quad (16)$$

where $E_{ac,rms} = E_{ac}(2)^{-1/2}$. Linear electromigratory phenomena can be neglected if the ac to dc ratio, α, is high, because the nonlinear, dielectrophoretic term will dominate. In contrast, both linear and nonlinear effects must be retained at dc (when α is equal to zero), owing to the presence of spatial variation in the electric field.

(1) Electric Field Solution. In order to achieve continuous-flow particle separation, we modulate electric potential in three dimensions. Accordingly, the complete solution for the electric potential is a three-dimensional field that can be approximated through numerical analysis by solving

$$\nabla\cdot d^*\nabla\phi^* = 0 \quad (17)$$

where d refers to local channel depth and asterisks denote nondimensionalized parameters. This is a modified Laplace equation, discussed by Cummings and Singh,[26] that is computationally inexpensive and allows us to obtain a 3D solution by parametrizing the third dimension and solving the resulting 2D equation. We take the gradient of potential, redimensionalize, and use this solution as $\vec{E}_{dc}$. We then apply eq 14 to model particle motion.

In order to model the effects of various geometric factors, we use a set of simplified solutions, which garner physical insight and allow straightforward comparison between experimental observations and simulated results. We consider two particular cases: (i) an applied potential gradient normal to an infinitely long constriction in channel depth, which results in particle stagnation and trapping, and (ii) an infinitely long constriction in channel depth at an angle to the applied potential (Figure 1b), which results in particle motion tangent to the constriction. The normal direction is defined on the *x*-axis in the side view of Figure 1b and perpendicular to the constriction region in the *x*−*y* plane of the top view in Figure 1b. The tangential direction is defined as parallel to the constriction region in the top view of Figure 1b or tangent to the curvature of the constriction at a given point in the *x*−*y* plane in Figure 1a.

(2) Particle Stagnation and Trapping. Particle motion in the presence of an infinitely long constriction in depth normal to the applied potential is simulated with two-dimensional techniques and mimicked experimentally with straightforward 2D fabrication as a constriction in channel width. This allows direct comparison between simulation and experiment, which leads us to a straightforward linearization that aids extension of our 2D engineering model to three dimensions.

Device operation involves tuning the ac to dc ratio α so that particle motion normal to the ridge is eliminated, causing particles to be deflected by surface ridges in a manner that leads to continuous-flow sorting. We therefore develop relations in this section that specify the α required to stagnate particles at a specific location (α_s) and the α required to stagnate all of the particles in a cross section of the flow (α_d). The α_d relation, applied normal to a ridge, defines the α required to cause particles to be deflected and sorted by surface ridges.

The ac to dc ratio α_s required to locally eliminate the particle velocity component in the x_i direction is a scalar field and can be found by taking the x_i component of eq 14 and setting the result equal to zero:

$$\alpha_s = \sqrt{-\frac{\hat{x}_i\cdot\vec{E}_{dc}}{(\partial/\partial x_i)(\vec{E}_{dc}\cdot\vec{E}_{dc})}\frac{\mu_{EO} + \mu_{EP}}{\mu_{DEP}} - 2} \quad (18)$$

This condition specifies local particle stagnation in a specific direction owing to offsetting contributions from the linear and nonlinear electromigratory effects. A particle is deflected by the surface ridge when its instantaneous velocity normal to the ridge is zero. α_s is small only in regions where the electric field gradients are high (i.e., near the edges of surface ridges), indicating that these regions are the locations where particles will be deflected at ac to dc ratios accessible to experiments.

Complete particle deflection requires that, at the experimental conditions, there be a surface that transects the flow on which particle motion normal to the ridge is zero. This condition can only be determined in general by solving the Laplace equation for the specified geometry (as noted in the previous section), determining the α required for such a surface to exist, and terming this result α_d. Similar trapping results have been observed and modeled by several researchers.[24,27,28] This exact solution can also be approximated by linearizing the gradient of the electric field magnitude squared:

$$\nabla(|\vec{E}|^2) \sim \frac{|E_r|^2 - |E|^2}{\gamma} \quad (19)$$

which captures the spatial variations of the electric field, approximately, via a shape factor γ (E_r is the electric field in the constriction region, $E_r \approx rE$). With this relation, the deflection ac to dc ratio α_d is approximated (for a ridge normal to the electric field) by

$$\alpha_d \sim \sqrt{\frac{1}{|\vec{E}_{dc}|}\frac{\mu_{EO} + \mu_{EP}}{\mu_{DEP}}\frac{\gamma}{(r^2 - 1)} - 2} \quad (20)$$

Later results will show that γ is only weakly dependent on ridge height and width and thus serves as a useful parameter for

(26) Cummings, E. B.; Singh, A. K. *Anal. Chem.* **2003**, *75* (18), 4724−4731.

(27) Lapizco-Encinas, B. H.; Simmons, B. A.; Cummings, E. B.; Fintschenko, Y. *Anal. Chem.* **2004**, *76* (6), 1571−1579.

(28) Tegenfeldt, J. O.; Prinz, C.; Cao, H.; Huang, R. L.; Austin, R. H.; Chou, S. Y.; Cox, E. C.; Sturm, J. C. *Anal. Bioanal. Chem.* **2004**, *378* (7), 1678−1692.

engineering design. α_d facilitates comparison between numerically simulated and experimentally observed particle behavior.

This representation allows us to clearly deliniate three parameters of interest: $1/|\vec{E}_{dc}|$, the applied electric field, which is an experimental input; $\gamma/(r^2 - 1)$, geometric factors, which are dictated by the channel geometry; and $(\mu_{EO} + \mu_{EP})/\mu_{DEP}$, the mobility ratio, which we are interested in measuring.

The mobility ratio captures electroosmotic, electrophoretic, and dielectrophoretic mobilities, and sorting by this ratio is useful in the biological systems of interest because the perturbations that we are concerned with predominantly affect the DEP mobility rather than electrophoretic mobility.[3,29,30]

(3) Particle Sorting. The particle stagnation and trapping described in the previous section allows for batch concentration of particles, but not continuous-flow sorting; however, since constrictions in this device are in depth, the geometry allows for another degree of freedom: the angle of incidence. By varying the angle of incidence of the channel constriction spatially, the DEP effects can be used to generate continuous particle sorting. Equation 20, above, states that a particle will be repelled from the constriction region by DEP forces perpendicular to the cross section of a constriction in depth. Applying this description to an angled constriction, we can decompose the bulk electric field and the electric field in the constriction region into normal and tangential components and in the process introduce a dependence on the constriction angle, θ (Figure 1b). As we did for the 2D stagnation case, we can define a local deflection ac to dc ratio based on the normal components of the electric field, by setting the normal particle velocity to zero:

$$\alpha_s = \sqrt{-\frac{\hat{n}\cdot\vec{E}_{dc}}{\frac{\partial}{\partial n}(\vec{E}_{dc}\cdot\vec{E}_{dc})}\frac{\mu_{EO}+\mu_{EP}}{\mu_{DEP}} - 2} \qquad (21)$$

Linearizing the gradient term as before, α_d from above becomes

$$\alpha_d \sim \sqrt{\frac{1}{|\vec{E}_{dc}|}\frac{\mu_{EO}+\mu_{EP}}{\mu_{DEP}}\frac{\gamma}{(r^2-1)\cos\theta} - 2} \qquad (22)$$

For a normal ridge, $\theta = 0°$, and we recover the 2D solution.

We briefly examine the case of two otherwise identical particles with different μ_{DEP} introduced to the same device under identical experimental conditions. We can compare the deflection angles of these particles by equating α_d for the two cases.

$$\cos\theta_2 = \cos\theta_1\frac{\mu_{DEP,1}}{\mu_{DEP,2}} \qquad (23)$$

The scaling relationships developed in eqs 20 and 22 are important simplifications that allow us to make qualitative predictions regarding the behavior of particles and engineer channel geometries that efficiently accomplish our goal of designing a continuous-flow particle sorting device. Later, we show that these simplifications are supported by experimental data.

As suggested by eq 22, the point at which particles pass the curved ridge is uniquely dependent on the ratio of a particle's electrophoretic and electroosmotic mobilities to dielectrophoretic mobility. By varying the angle of incidence, we modulate the dielectrophoretic component of velocity and couple DEP mobility to transverse position, effectively sorting particles by their mobility ratio. Equation 20 allows us to rationally design the constriction ratio of the device such that values of α_d lie within the operability range of our experimental apparatus. Equation 22 also suggests that the output distribution of particles is a continuous function of DEP mobility, rather than a binary or otherwise discretized output.

MATERIALS AND METHODS

Device Fabrication. Device geometries were defined using L-Edit CAD software (Tanner Research). Two mask patterns were created for different etch depths: one to define the channel itself and one to define a pattern of ridges in the channel. Masks were created using standard protocols using a GCA/MANN 3600F Optical Pattern Generator and processed with a Hamatech-Steag HMP900 Mask Processor. P-type [100] silicon wafers with 1000 nm of thermal oxide (University Wafer) were coated with Shipley 1813 photoresist, spun at 3000 rpm for 30 s and placed on a hot plate (115 °F) for 1 min. The wafer was then exposed using the ridge mask in soft contact using an EV 620 (EV Group) alignment tool. Resist was developed in a Hamatech-Steag Wafer processor with 300MIF developer for 1 min. The thermal oxide was then chemically etched using 6:1 buffered oxide etch for 15 min. The wafer was then cleaned and the resist stripped. The wafer was recoated and the channel outline pattern exposed. The resist was again developed using 300MIF resist developer and thermal oxide etched again. After this step, oxide covers only the regions of the wafer that correspond to regions of full depth; resist covers regions of features in the channel. The wafer was then etched using a Unaxis SLR 770 Bosch etch tool to the desired feature depth. Resist was stripped and the wafer was etched a second time, to the desired channel depth. Remaining thermal oxide was then removed. The wafer was then glued to a glass back for use as a device master.

We have designed and fabricated functional microfluidic devices in polymeric substrates with aspect ratios (250:1) and depths (100 μm), higher than previously reported.[31,32] Fabrication was based on procedures (adapted from Esch et al.[31] and Wallow et al.[32]) that employ hot embossing and chemical bonding of Zeonor thermoplastic devices. Plaques of Zeonor 1020R cycloolefin copolymer substrate (Zeon Chemicals) were cut using a band saw into 1.5-in.-square chips. The silicon device master and a Zeonor chip were aligned and placed in a hot press (Fortin CRC Prepreg), and 1000 lb of force was applied at 240 °F. The set point temperature was immediately decreased to 195 °F, and the chip was allowed to cool under load (30 min). After the device was removed from the press, access holes were drilled using a drill

(29) Smeulders, M. J.; Keer, J.; Speight, R. A.; Williams, H. D. *J. Bacteriol.* **1999**, *181* (1), 270−283.
(30) Lytle, D.; Frietch, C.; Covert, T.*Appl. Environ. Microbiol.* **2004**, *70* (9), 5667−5671.
(31) Esch, M. B.; Kapur, S.; Irizarry, G.; Genova, V. *Lab Chip* **2003**, *3*, 121−127.
(32) Wallow, T. I.; Morales, A. M.; Simmons, B. A.; Hunter, S. M.; Krafcik, M. C.; Domeier, K. L.; Sickafoose, L. A.; Patel, G. A.; Gardea, A. *Lab Chip*. Submitted.

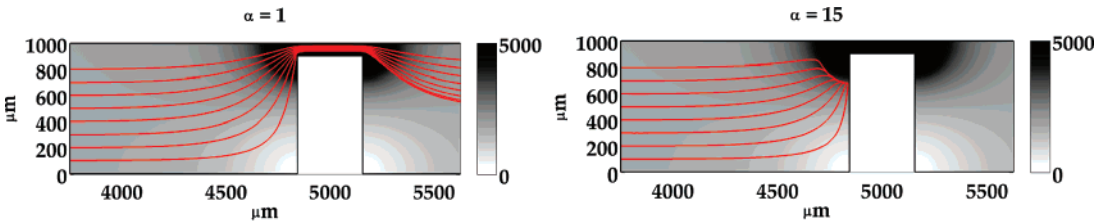

(a) Simulation for $\alpha = 1$. (b) Simulation for $\alpha = 15$.

Figure 2. Simulated particle streamlines (red line) for high and low ac to dc ratios. Background color table corresponds to electric field magnitude. Simulation parameters: $\phi_{inlet} = 50$ V, constriction ratio 10:1, particle radius 1 μm.

press and a 1-mm end mill at 620 rpm to prevent burring and melting. The Zeonor chip was then treated in a solution of 20% (v) *cis*− *trans*-decahydronaphthalene (Sigma Aldrich) and 80% (v) ethyl alcohol for 30 s. Another, blank, Zeonor chip was treated in the same solution for 1 min. Both were cleaned with ethyl alcohol and dried using compressed nitrogen. The pieces were then immediately placed and aligned in the hot press for bonding. Poly(dimethylsiloxane) (PDMS) backing on both sides was used to correct for any deviations in the flatness of the press. PDMS backing material was fabricated using a standard Sylgard 184 Elastomer kit (Dow Corning) and a 5:1 ratio of elastomer to curing agent. After curing, channel-shaped holes were cut into the PDMS and aligned with the device in press so that pressure from the press is applied only in regions away from access holes. Bonding was carried out at 140 °F, 356 lb force for 40 min, and the PDMS backing removed.

Reservoirs were fashioned out of 1000-μL pipet tips and bonded to the Zeonor plaque using chloroform.

Particle Experiments. Channels were first filled with isopropyl alcohol to facilitate the removal of air bubbles. Deionized water (pH 7) was then run through the devices using positive pressure several times to remove the isopropyl alcohol. The 1.75- and 2-μm FluoresBrite (Polysciences) and 3-μm Fluosphere (Molecular Probes, Invitrogen) carboxylate-modified fluorescent polystyrene spheres were introduced in the form of a 100:1 diluted solution of deionized water and spheres. The 1.75-, 2-, and 3-μm spheres fluoresce (emit) at different spectra (486, 486, and 415 nm, respectively) and were observed using a X-Cite 120 fluorescent source and a Nikon TE2000U inverted microscope. Images and movies were obtained using a Q-Imaging Retiga EXi FAST camera and Phylum software. Image analysis was carried out in MATLAB (MathWorks).

Throughout all experiments, extreme care was taken to eliminate pressure-driven flow by equalizing reservoir heights. Observation of stagnant particles was used as an indicator of pressure equalization.

Electric potentials were generated using an Agilent 33220A arbitrary waveform generator and amplified with a Matsusada Precision AP/AS amplifier. Potentials were applied to reservoir solutions through pure platinum electrodes to minimize electrolytic products and measured with a HP 54501A digital oscilloscope. *Caution! High voltage can lead to injury.* Take appropriate precautions when working with high voltage systems. Wear rubber gloves and never touch leads while the power supply is on. Make sure all equipment is rated appropriately, and ensure that energized surfaces are safely separated from the user.

RESULTS

We conducted two sets of simulations and experiments. Taken together, these results (i) demonstrate continuous-flow particle sorting, (ii) show the effectiveness of the mobility model and approximations in predicting particle behavior, and (iii) provide tools for future engineering design of similar systems. First, we simulated a 2D geometry with a constriction in depth, using numerical techniques, and determined values for α_s as a function of constriction ratio, r, and constriction shape, γ. Experimentally, we mimicked this geometry with a similar constriction in channel width and measured α_d as a function of constriction ratio and shape. Second, we simulated a curvilinear constriction in channel depth, again using numerical techniques, and determined relative values of θ for different particles. Experimentally, we implemented the same geometry and introduced particles with different μ_{DEP} and measured deflection (θ). The resulting deflection in continuous flow allowed for particle separation that is a continuous function of μ_{DEP} and transverse channel position.

Particle Trapping. Simulated and experimental observation of the particle trapping response in the presence of a constriction in channel dimensions is consistent with the particle velocity model developed in eq 14. We assess the results of simulations and experimental results by comparing α_s values and fitting results with γ as a free parameter in eq 20.

(1) Simulation. Applying the 3D particle velocity model derived above and a 2D electric potential field solution to the microchannel geometry of interest, we can rapidly simulate particle trapping behavior in the presence of a constriction in channel depth. Equation 14 predicts that particles will experience deflection in the presence of the constriction, and will pass through the constriction region for low values of α (Figure 2a) while being excluded from the constriction region for high values of α (Figure 2b). Simulations were conducted in parametric fashion, varying the constriction ratio, r, from 2 to 20, and the width of the ridge over 1 order of magnitude (10−100 μm). The determination of the trapping ac to dc ratio, α_s, according to eq 18, was made by examining particle velocity in the x-direction at $y = 1000$ μm (Figure 2). This ensures that when $u_x \leq 0$, particles are completely excluded from the constriction region, defining the trapping threshold for that system. A range of channel constrictions were considered ($2 \leq r \leq 20$), and the simulated data were fit by allowing γ to vary in eq 20.

Simulations show that the width is not a significant factor in determining α_s. The geometric factor, γ, shows small variation as a function of width. ac to dc ratios show a strong dependence on the constriction ratio and vary in a manner consistent with

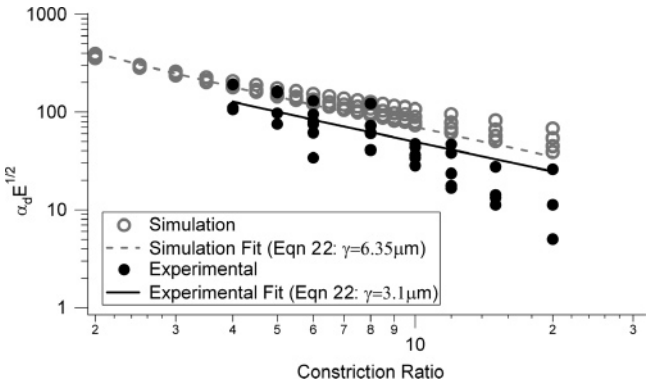

Figure 3. Simulated and experimental values of $\alpha_d(E_{dc}^{1/2})$ show good fit quality and expected dependence on r and γ. Multiplication of α_d by $E_{dc}^{1/2}$ emphasizes the dependence of α_d on factors determined by channel geometry (γ and r) and eliminates the dependence of α_d on E_{dc}. Scatter in simulated data points is attributable to minor effects of constriction width. Applied (dc) electric fields are either 25 or 50 V/cm in simulation and experiment, electric field frequency is 1 kHz, and particle size is 2 μm.

the scaling arguments presented in eq 20. R^2 values for the model fit (with the parameter γ) to simulated α_s are $\geq$0.90 (Figure 3).

(2) Experiment. Microfluidic channels were fabricated in Zeonor 1020R polymer with constrictions in width, corresponding to variations in constriction ratio in simulated geometries. Subsequently, the motion of 2-μm-diameter polystyrene spheres was observed at increasing ac to dc ratios. α_s values where particles were excluded from the constriction region were recorded and compared to those predicted from 3D analytical results and 2D simulation. Comparison between experimental values of α_d and those predicted by eq 18 show similar trends (Figure 3), evidenced by the quality of γ fitting ($R^2 = 0.9$). Values of α differ between simulation and experiment, but trend heavily with the constriction ratio, as expected from eq 18, confirming its status as a critical design parameter. The difference in γ values for simulation and experiment stems largely from the comparison of 2D simulation data to 3D experimental data. However, the similar scaling between theory, simulation, and experiment supports the use of eq 20 and the associated engineering approximations as a valid design tool for future work.

Single-Particle Deflection. We observe particle deflection along an angled ridge in simulation and experiment by varying the ac to dc ratio, α. This is predicted by the particle velocity model, from the section Particle Stagnation and Trapping

(1) Simulation. Particle deflection behavior (i.e., particle motion along an angled ridge) was simulated by applying the 3D particle velocity model and a quasi-2D electric potential field solution technique to the microchannel geometry of interest. The geometry of interest is a curved constriction in channel depth described in the section Particle Sorting and Figure 1. Using eq 14, derived above, and a numerical solution for eq 17 over the geometry of interest, we simulate particle motion in the presence of a curved constriction in channel depth. Appropriate redimensionalization requires values for particle and wall zeta potentials, which we obtain through light scattering (Malvern Zetasizer) and streaming potential measurements[24,33,34] ($\zeta_{particle} = -60$ mV and $\zeta_{wall} = -40$ mV, respectively). The Clausius−Mossotti factor, f_{CM}, for these particles is assumed to be well-approximated by −0.5 in the low-frequency limit, since $\sigma_{polystyrene} \ll \sigma_{fluid}$. Plotting particle pathlines from the velocity solution, we show that particle deflection along the y-axis is dependent on the ac to dc ratio, α, as described above (Figure 4).

(2) Experiment. A microchannel with a curved constriction in channel depth was fabricated, and particle deflection along the y-axis as a function of the ac to dc ratio was observed. The degree of transverse (y-axis) deflection as a function of θ and α was characterized by measuring time lapse ($\geq$30 frames, Figure 4c) fluorescence image intensity along the y-axis at the channel outlet and computing a running integral of image intensity. Curves for several ac to dc ratios compare the degree of deflection and demonstrate the predicted dependence of deflection on the ac to dc ratio, α (Figure 4d). The cumulative distribution function is computed as a running integral of normalized image intensity and corresponds to a fraction of total positioned particles existing above a specified y-axis position.

Particle Separation. Particle deflection behavior in continuous flow is dependent on individual particle characteristics, specifically, the ratio of linear to nonlinear electrokinetic mobilities (eq 21).

(1) Simulation. Particle deflection behavior is controlled by the magnitudes of the dc and ac electric field components (E_{dc} and E_{ac}) and is dependent on a number of particle-specific properties that determine the electrophoretic and dielectrophoretic mobilities. Based on this dependence, we predict particle sorting behavior that is a function of differences in the ratio of dielectrophoretic to electrophoretic and electroosmotic mobilities. A dimensional simulation, carried out as described in the section Electrical Field Solution, for a constant ac to dc ratio, shows deflection that is dependent on particle size (Figure 5a and b).

(2) Experiment. Separation of 2- and 3−μm particles was accomplished in continuous flow using the device shown in Figure 1. As described above, deflection can be characterized by calculating a cumulative distribution function from time lapse fluorescence intensity at the channel outlet. The intensity of each particle population (2 and 3 μm) was independently measured and normalized prior to comparison. Figure 5 shows particle separation from a localized input stream of mixed particles. The degree of deflection of both particles can be modulated by changing the ac to dc ratio or field magnitudes. At lower values of α, 2-μm particles remain at the top of the channel while 3-μm particles are deflected. If α is increased, the deflection of 3-μm particles continues to increase until they reach the bottom of the channel. Deflection of 2-μm particles can then be modulated by further adjustment of α.

DISCUSSION

We have demonstrated (i) continuous-flow separation of particles, (ii) agreement between theory, simulation, and experiment, and (iii) simple modeling relationships for engineering design. Particle deflection and trapping were shown to be functions primarily of constriction ratio with minor contributions from other geometric factors.

The use of dc-offset, ac electric fields allows independent modulation of linear electromigratory effects and nonlinear di-

(33) Kirby, B. J.; Hasselbrink, E. F. *Electrophoresis* **2004**, *25*, 187−202.

(34) Kirby, B. J.; Hasselbrink, E. F. *Electrophoresis* **2004**, *25*, 203−213.

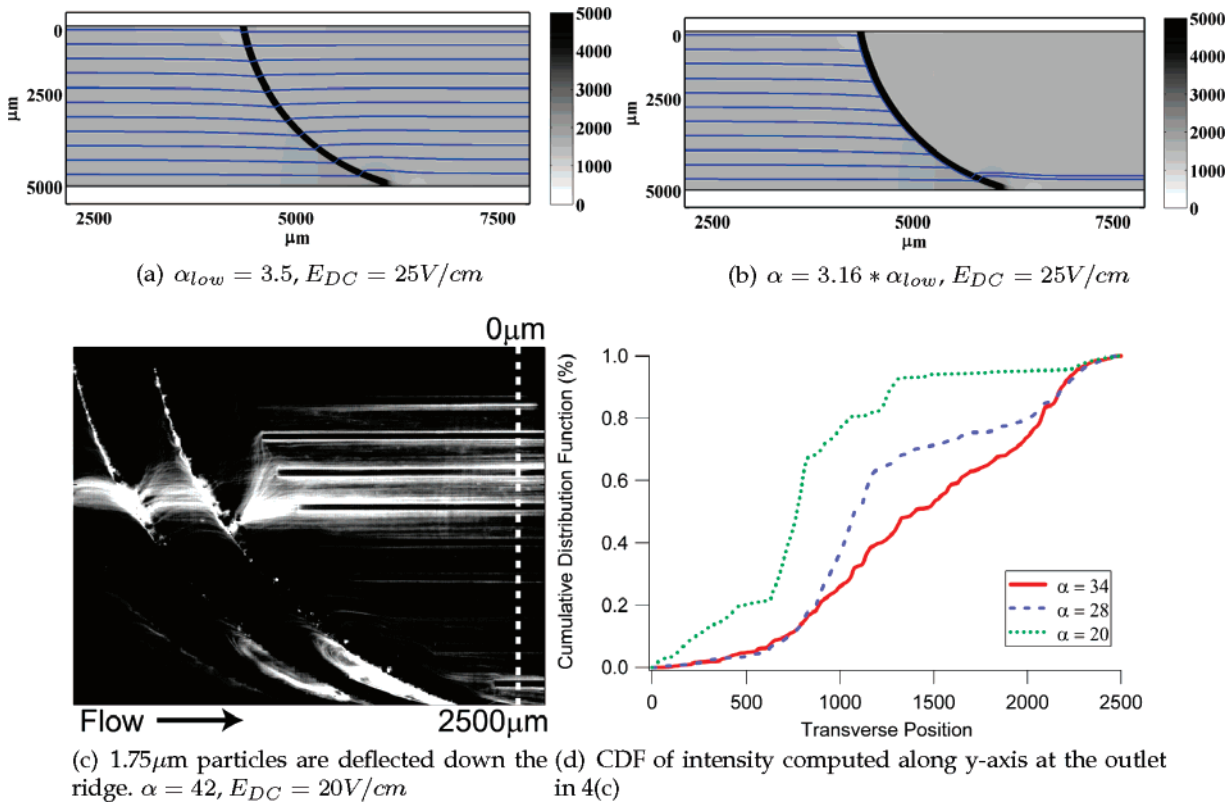

Figure 4. Varying the ac to dc ratio, α, increases transverse (*y*-axis) deflection. Simulated particle pathlines in (a) show no net particle deflection at a low ac to dc ratio. (b) shows particle deflection tangent to a curved constriction in channel depth, transverse to the direction of flow for a high ac to dc ratio. Simulated particle radius of 1 μm. Electric field frequency is 1 kHz.

electrophoretic effects. The addition of a dc-offset allows precise control of fluid and particle motion and avoids the use of pressure-driven flow. Direct current electric fields can actuate the nonlinear effects utilized in this work, but in general, higher field strengths would be required, increasing the likelihood of interference from heating and electrolysis. An ac field alone would require the use of pressure to actuate fluid and particle motion, which, in turn, would introduce a nonuniform flow field around the channel constrictions. Additionally, the addition of pressure-driven flow breaks the similitude between fluid velocities and electric fields used to model this system.[35] By combining ac and dc fields, we gain the ability to precisely actuate fluid motion and independently modulate nonlinear DEP effects without sacrificing modeling or experimental simplicity.

The sorting demonstrated in this work is dependent on linear and nonlinear electrokinetic mobilities, which are a function of cell size and electrophoretic mobility, and will affect device performance. By using EP mobility and size distribution measurements to define operating parameters, viable separation based on DEP mobility can be accomplished. For an isolated bacterial cell sample, size and EP mobility often vary little.[3,29,30] In future work, we are interested in developing a high-throughput screening technique for membrane-specific phenotypic differences in a single bacterial species, where we can assume a narrow distribution of size and electrophoretic mobility.

While insulator-based dielectrophoretic techniques have been reported by others, to the authors knowledge, this is the first reported use of 3D device geometries for continuous-flow particle processing by iDEP. Chou et al. reported the use of iDEP at low field frequencies to trap single- and double-stranded DNA in an array of insulating posts.[36] Similarly, Lapizco-Encinas et al. reported the use of iDEP and dc electric fields to trap and distinguish bacterial species[37] and to separate live from dead bacteria.[27] Mela et al. reported similar results using a polymeric post array.[24] Trapping and binary separation techniques such as these have the advantage of robust operation and ease of fabrication, but typically require higher electric fields than electrode-based techniques to generate similar electric field gradients. Additionally, obtaining separated samples is frustrated by the fact that samples are separated temporally in a flow, rather than spatially. Cummings and Singh reported the use of dc electric fields in an array of insulating posts with different angles of incidence to the direction of flow.[22,26] The result is a spatial separation based on accumulation of DEP effects over all post constrictions in the array. Similarly, this technique requires high electric fields to generate gradients, but achieves spatial sample separation, albeit over the length of the post array. Kang et al. reported the separation of particles based on size over a "hurdle" in the channel.[18] This hurdle is analagous to the constriction described above. By applying a dc electric field, the hurdle causes a net change in the particle trajectory,[19] which was used to separate particles with a significant difference in size. The separation described by Kang et al.,[18]

(35) Cummings, E. B.; Griffiths, S. K.; Nilson, R. H.; Paul, P. H. *Anal. Chem.* **2000**, *72* (11), 2526−2532.

(36) Chou, C. F.; Tegenfeldt, J. O.; Bakajin, O.; Chan, S. S.; Cox, E. C.; Darnton, N.; Duke, T.; Austin, R. H. *Biophys. J.* **2002**, *83* (4), 2170−2179.

(37) Lapizco-Encinas, B. H.; Simmons, B. A.; Cummings, E. B.; Fintschenko, Y. *Electrophoresis* **2004**, *25* (10−11), 1695−1704.

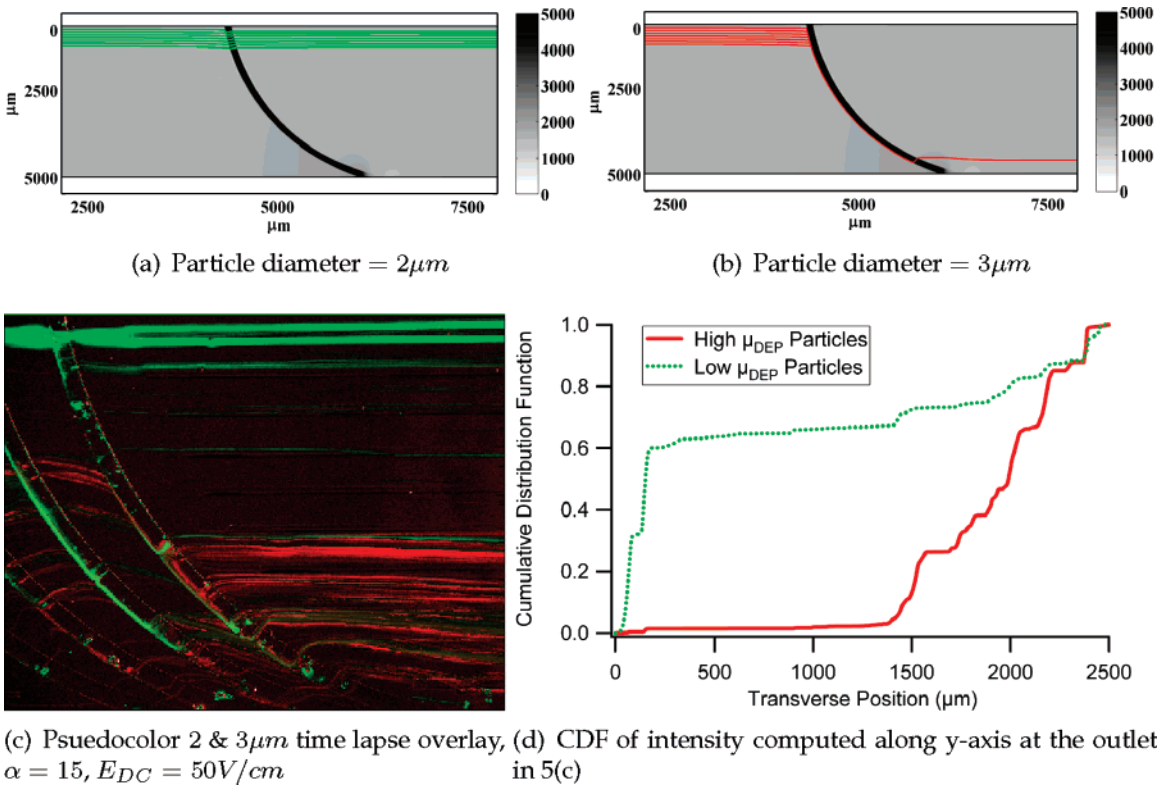

Figure 5. The 2-μm particles passing the ridge with no net *y*-axis deflection. The 3-μm particles show significant net *y*-axis motion as expected due to higher DEP mobility. Background color table in (a) and (b) represents $|E_{dc}|$. Simulation parameters: $\phi_{inlet} = 50$ V, constriction ratio $r =$ 10:1, and $\alpha = 15$. Experimental parameters: $\phi_{inlet} = 50$ V, $\alpha = 5$. Electric field frequency is 1 kHz.

depends on the variation of particle trajectories as they pass the hurdle. By relying on exclusion from the constriction region rather than changes in trajectory, the device reported above achieves more robust operation while maintaining a continuous sensitivity to particle mobilities.

Electrode-based DEP trapping techniques are well established, and new electrode and device geometries continue to be developed.[3] Work on the characterization of multipolar electrode arrays for DEP trapping and analysis has been presented by Voldman and co-workers.[11−13] The use of multipolar and 3D electrode configurations to trap cells has been investigated extensively by Fuhr and co-workers.[5−10] While these trapping techniques are ideal for particle characterization and interaction studies, continuous-flow techniques that act on many particles simultaneously offer significantly higher separation throughput.

We present continuous-flow, insulative dielectrophoresis using dc-offset, ac electric fields, in contrast to similar devices, which achieve continuous-flow separation using microfabricated, in-channel electrodes in the place of a curved ridge[23,38] or straight insulative constrictions in channel depth.[20,21] Kralj et al. demonstrated continuous-flow particle separation using an array of angled electrodes to direct particles into one of two outputs based on DEP mobility.[23] Barrett et al. fabricated a channel in glass that contains an angled constriction in channel depth. Both devices achieve a binary separation based on the ratio of DEP to EO and EP mobilities. Schnelle et al.[38] fabricated a microchannel containing curved electrodes on top and bottom of the device. The curved electrodes operate using the same mechanism as the constriction described here; trapping between dielectrophoretic and fluid drag forces occurs at the electrode and is dependent on the angle between the electrode and the direction of fluid flow.[38] By using polymeric substrates, 3D geometries, and dc-offset, ac electric fields, we reduce the cost and difficulty of manufacture, achieve a continuous (rather than discrete) separation, precisely actuate fluid flow using electroosmosis, and introduce increased experimental flexibility by changing the applied field frequency.

CONCLUSION

To the authors' knowledge, this is the first reported use of 3D, insulative techniques to effect a continuous-flow particle separation whose output is characterized by continuous variation of dielectrophoretic mobility perpendicular to the direction of flow. To interpret the data, we developed a set of theoretical approximations to be used in the design of similar microfluidic systems for the manipulation of particles using insulative dielectrophoresis, coupled with electrophoresis and electroosmosis for fluid and particle transport. We applied this model to the design and development of continuous-flow dielectrophoretic sorting devices with 3D modulation of electric fields. Theoretical and experimental results were compared by measuring the trapping threshold value, α_s, in simulation and experiment. Measurement of α_s is a straightforward method of characterization compared to tracking single particles or a statistical average of particles, and applies directly to the particle sorting device (Figure 1b). Device fabrication achieves aspect ratios higher than previously reported for bonded thermoplastic devices (250:1, width to depth). Device functionality was verified by sorting 2- and 3-μm polystyrene

(38) Schnelle, T.; Muller, T.; Gradl, G.; Shirley, S. G.; Fuhr, G. *J. Electrostat.* **1999**, 47, 121−132.

spheres with similar material and surface properties. Model, simulation, and experiment showed similar trends. The advantage of 3D modulation of electric fields is the resulting continuous variation of particle mobility ratios transverse to the direction of flow. This output can be separated into any number of output channels, yielding the potential for unprecedented resolution for a single separation.

ACKNOWLEDGMENT

The authors acknowledge the valuable input of Blake Simmons, Sandia National Laboratories, in the development of polymer fabrication techniques, and Eric Cummings, Sandia National Laboratories, in conceptual design. B.G.H. and A.E.S contributed equally to this work.

NOTE ADDED AFTER ASAP PUBLICATION

The article was posted on the web on 8/30/07. Typographical errors in eq 3 and a few variables were corrected. The paper was reposted on 9/12/07.

Received for review April 12, 2007. Accepted June 28, 2007.

AC0707277